



# Overexpression and kinetic analysis of *Ideonella sakaiensis* PETase for polyethylene terephthalate (PET) degradation

Lizhu Aer<sup>a</sup>, Qifa Jiang<sup>a</sup>, Ijaz Gul<sup>a,b</sup>, Zixuan Qi<sup>a</sup>, Juan Feng<sup>a,c</sup>, Lixia Tang<sup>a,c,\*</sup>

<sup>a</sup> School of Life Science and Technology, University of Electronic Science and Technology of China, Chengdu, 610054, China

<sup>b</sup> Institute of Biopharmaceutical and Health Engineering, Tsinghua Shenzhen International Graduate School, Tsinghua University, Shenzhen, 518055, PR China

<sup>c</sup> Center for Informational Biology, University of Electronic Science and Technology of China, Chengdu, 610054, China

## ARTICLE INFO

### Keywords:

IsPETase  
Expression optimization  
GroEL/ES co-Expression  
NusA fusion system  
Biodegradation of PET

## ABSTRACT

*Ideonella sakaiensis* PET hydrolase (*IsPETase*) is a well-characterized enzyme for effective PET biodegradation. However, the low soluble expression level of the enzyme hampers its practical implementation in the biodegradation of PET. Herein, the expression of *IsPETase*<sup>Mut</sup>, one of the most active mutants of *IsPETase* obtained so far, was systematically explored in *E. coli* by adopting a series of strategies. A notable improvement of soluble *IsPETase*<sup>Mut</sup> was observed by using chaperon co-expression and fusion expression systems. Under the optimized conditions, GroEL/ES co-expression system yielded  $75 \pm 3.4$  mg·L<sup>-1</sup> purified soluble *IsPETase*<sup>Mut</sup> (GroEL/ES), and NusA fusion expression system yielded  $80 \pm 3.7$  mg·L<sup>-1</sup> purified soluble NusA-*IsPETase*<sup>Mut</sup>, which are 12.5- and 4.6-fold, respectively, higher than its commonly expression in *E. coli*. The two purified enzymes were further characterized. The results showed that *IsPETase*<sup>Mut</sup> (GroEL/ES) displayed the same catalytic behavior as *IsPETase*<sup>Mut</sup>, while the fusion of NusA conferred new enzymatic properties to *IsPETase*<sup>Mut</sup>. Although NusA-*IsPETase*<sup>Mut</sup> displayed a lower initial hydrolysis capacity than *IsPETase*<sup>Mut</sup>, it showed a 1.4-fold higher adsorption constant toward PET. Moreover, the product inhibition effect of terephthalic acid (TPA) on *IsPETase* was reduced with NusA-*IsPETase*<sup>Mut</sup>. Taken together, the latter two catalytic properties of NusA-*IsPETase*<sup>Mut</sup> are more likely to contribute to the enhanced product release by NusA-*IsPETase*<sup>Mut</sup> PET degradation for two weeks.

## 1. Introduction

Polyethylene terephthalate (PET) is a polymer synthesized from terephthalic acid (TPA) and ethylene glycol (EG). It is widely used in both industry and our daily life due to its excellent properties for usage (Gao et al., 2021). In the last two decades, the demand for PET-based plastics has significantly increased, and in 2020 it exceeded 400 million tons (Skoczinski et al., 2021). Since most oil-based plastics are biodegradation-resistant and take a long time to degrade, the accumulation of plastic waste is anticipated to reach 33 billion tons by 2050 (Rochman et al., 2013), posing serious environmental problems. In addition to their presence in both soil and water, microplastics have also been found in marine animals, indicating the possibility of entering the human body through the food chain and posing a serious threat to human health (Chae et al., 2018; Hahladakis et al., 2018; Pabortsava and Lampitt, 2020; Zhang et al., 2018). Thus, plastic degradation is one of the most urgent problems that needs to be solved.

Currently, both chemical and physical treatments are still the two mainstreams for PET degradation (Day et al., 1982; Zope and Mishra, 2008). However, both methods are energy-consuming and environmentally unfriendly. Biodegradation has garnered substantial attention over the last two decades as it is an efficient and green approach for PET degradation. Till now, several PET-degrading enzymes, including lipase, carboxylesterase, cutinase and PETase have been isolated from bacteria and fungi (Danso et al., 2018; Eberl et al., 2009; Herrero Acero et al., 2011; Wei and Zimmermann, 2017). Among these enzymes, PETase isolated from *Ideonella sakaiensis* (termed as *IsPETase*) exhibits a great potential in PET degradation due to its relatively high activity compared to the other PET-degrading enzymes at room temperature (Table S1). In order to gain more insight into the molecular basis of its catalytic function, the X-ray structure of *IsPETase* has been solved recently by several groups (Austin et al., 2018; Han et al., 2017; Joo et al., 2018). Compared to its homologous enzyme *TfCut2* from *Thermobifida fusca*, *IsPETase* has a shallow and wide hydrophobic "L" shaped groove located

\* Corresponding author. School of Life Science and Technology, University of Electronic Science and Technology of China, No. 4, Section 2, North Jianshe Road, Chengdu, China.

E-mail address: [lixitang@uestc.edu.cn](mailto:lixitang@uestc.edu.cn) (L. Tang).

on the protein surface, allowing it to interact with aggregated PET substrate, while the substrate-binding cleft of *TfCut2* is narrow and deep without forming a continuous cleft (Joo et al., 2018). In addition to its unique binding site, *IsPETase* was proved to have a more flexible active-site at room temperature than its thermophilic counterparts, all of which might be the key factors explaining why *IsPETase* could accommodate a bulkier substrate like PET at room temperature (Fecker et al., 2018; Liu et al., 2018). Further understanding of the nature of the high activity of *IsPETase* at room temperature is still needed. Moreover, all this structural information greatly aided in the improvements of *IsPETase* activity and stability via rational and semi-rational modification strategies (Austin et al., 2018; Chen et al., 2018; Joo et al., 2018; Liu et al., 2018; Meng et al., 2021; Puspitasari et al., 2021; Son et al., 2019).

To facilitate the application of *IsPETase* for the biodegradation of PET, the extracellular secretion of the enzyme has enticed substantial research attention. The secreted expression of *IsPETase* has been conducted in several organisms, including *Bacillus subtilis*, *Escherichia coli*, *Pichia pastoris* GS115, and even *Chlamydomonas reinhardtii* and microalgae (Chen et al., 2020; Huang et al., 2018; Kim et al., 2020; Moog et al., 2019; Seo et al., 2019; Wang et al., 2020; Xi et al., 2021). Since *E. coli* is a frequently used host cell for the production of recombinant proteins due to its fast growth, low cost, high productivity, and well characterized genetic background, the enhancement of the secretion of *IsPETase* was further explored in *E. coli* by the selection of optimal translocation signal peptides from *E. coli* (Seo et al., 2019). More recently, engineering of a Sec-dependent signal peptide of *pelB* was reported to improve the secretion of *IsPETase* in *E. coli*, resulting in up to 1.7-fold higher *IsPETase* secretion by using the evolved *pelB* (Shi et al., 2021).

Although much effort has been devoted to the secretion production in *E. coli*, their soluble expression levels are still low and not suitable for the production of *IsPETase* on a large-scale. To this point, cytoplasmic overexpression of *IsPETase* in *E. coli* could represent an alternative way to full fill the task. Thus, in this study the overexpression of *IsPETase*<sup>Mut</sup>, one of the most active mutants of *IsPETase* (Son et al., 2019), was fully explored in *E. coli*. For this, both strategies of co-expression with chaperones and the N-terminal tags fusion expression were adopted for the intracellular expression of *IsPETase*<sup>Mut</sup> in *E. coli*. After optimization, a 12.5- and 4.6-fold overexpression of soluble *IsPETase*<sup>Mut</sup> was achieved by using both the co-expression of chaperone GroEL/ES and the N-terminal NusA-tag fused expression, respectively, compared to its common expression in *E. coli*. The overexpressed mutants were then employed to the biodegradation of PET bottle. To the best of our knowledge, we report the highest soluble expression level of *IsPETase* in *E. coli*. Moreover, NusA confers new catalytic properties to *IsPETase*<sup>Mut</sup>, endowing the enzyme with a high catalytic efficiency in the long-term biodegradation of PET. Our study introduces a more efficient recombinant *IsPETase*<sup>Mut</sup> production process and provides kinetic investigations of the resulting enzymes on PET degradation.

## 2. Materials and methods

### 2.1. Materials

Bis (hydroxyethyl) terephthalate (BHET) and terephthalic acid (TPA) were purchased from Sigma-Aldrich. Hydroxyethyl terephthalate (MHET), isopropyl β-D-thiogalactoside (IPTG), kanamycin, and chloramphenicol were purchased from Solarbio Biotechnology Co., Ltd. (Beijing, China). All restriction endonucleases, high-fidelity plasmid DNA polymerase, *DpnI*, T4 DNA ligase and protein thermal shift dye (Applied Biosystems) were obtained from Thermo Fisher Scientific Co., Ltd. (Chengdu, China). The two parts of commercial PET bottle were used as substrates in this study: the neck part termed as PET-NP with 9.4% crystallinity and the body part termed as PET-BP with 17.9% crystallinity. All gene synthesis and primer sequencing in the experiments were performed by Beijing Tsingke Biotechnology Co., Ltd. (Beijing, China). Vectors pBAD, pET30a, pKJ7, pGro7, pTF16 were

stored in our laboratory, *E. coli* Dh5α, shuffle-T7, Top10 competent cells were purchased from Solarbio Biotechnology Co., Ltd.

### 2.2. Expression vector construction

The *IsPETase*<sup>Mut</sup> gene was synthesized and cloned into the pBAD vector to obtain pBAD-*IsPETase*<sup>Mut</sup>. Using pBAD-*IsPETase*<sup>Mut</sup> as a template, the *IsPETase*<sup>Mut</sup> gene was amplified and inserted into the pET30a vector to obtain pET30a-*IsPETase*<sup>Mut</sup>. The sequences of *Sumo*, *NusA*, *Mbp* and *TrxA* genes were synthesized and cloned into pET30a-*IsPETase*<sup>Mut</sup> to obtain pET30-Sumo-*IsPETase*<sup>Mut</sup>, pET30-NusA-*IsPETase*<sup>Mut</sup>, pET30-Mbp-*IsPETase*<sup>Mut</sup> and pET30-TrxA-*IsPETase*<sup>Mut</sup>, respectively. All expression vectors and host cells are shown in Table S2.

### 2.3. Protein expression and purification

The pBAD-*IsPETase*<sup>Mut</sup> vector was transformed into *E. coli* Top10 competent cells, and *IsPETase*<sup>Mut</sup> expression was induced in 200 mL of LB medium with different induction temperatures and different concentrations of arabinose.

The three chaperone systems DnaK/DnaJ/GrpE, GroEL/ES and TF were co-expressed with *IsPETase*<sup>Mut</sup> in *E. coli* shuffle-T7, respectively. Briefly, *E. coli* shuffle-T7 competent cells were firstly transformed with plasmid carrying a chaperone system. The transformants were selected with a LB agar plate containing chloramphenicol, which were then used to generate chemical competent cells for the secondary transformation with the pET30-*IsPETase*<sup>Mut</sup> plasmid. Colonies carrying the above two plasmids were finally selected using LB agar plate containing double selection markers (chloramphenicol and kanamycin).

The expression of *IsPETase*<sup>Mut</sup> with pET30a constructs was carried out as follows: the expression vector was transformed into *E. coli* shuffle-T7 competent cells and cultured in 200 mL LB medium (after incubating OD<sub>600</sub> to 0.6–0.8 at 37 °C and 160 rpm, 1 mM IPTG was added and then expressed at 20 °C, 25 °C and 30 °C for 22 h) or 200 mL lactose self-induction medium (10 g·L<sup>-1</sup> peptone, 5 g·L<sup>-1</sup> yeast extract, 7.1 g·L<sup>-1</sup> Na<sub>2</sub>HPO<sub>4</sub>, 6.8 g·L<sup>-1</sup> KH<sub>2</sub>PO<sub>4</sub>, 3.3 g·L<sup>-1</sup> (NH<sub>4</sub>)<sub>2</sub>SO<sub>4</sub>, 0.5% (v·v<sup>-1</sup>) glycerin, 0.5 g·L<sup>-1</sup> glucose, 2 g·L<sup>-1</sup> lactose, 0.24 g·L<sup>-1</sup> MgSO<sub>4</sub>, ZYP) at 37 °C, 160 rpm for 2.5 h, then expressed at 20 °C, 25 °C and 30 °C for 22 h. Cells were harvested after centrifugation at 4000×g for 15 min, suspended in buffer A (50 mM Na<sub>2</sub>HPO<sub>4</sub>, pH 7.5 and 100 mM NaCl) and sonicated to break bacteria for 20 min (200 W, break 1 s stop 1 s). Cell debris was removed by centrifugation at 13500×g for 30 min, and the supernatant was purified by HisTrap column (GE Healthcare). The bound protein was washed with buffer A containing 30 mM imidazole and then eluted in buffer A with 300 mM imidazole, and the protein concentrations was determined by the Bradford method. Finally, HisTrap column-purified proteins were determined by size exclusion chromatogram using Superdex 200 Increase 10/300 GL columns (GE Healthcare).

### 2.4. Activity assays

The enzyme activity was monitored by using BHET (a soluble fragment of PET) as a model substrate for enzymatic characterization. BHET stock solution was made by dissolving 200 mg BHET in 10 mL dimethyl sulfoxide. The enzymatic reaction was performed at 30 °C for 30 min and was triggered by adding 50 nM purified enzymes in 0.6 mL reaction system (80 mM Na<sub>2</sub>HPO<sub>4</sub>-HCl, 40 mM NaCl, pH 7.5) containing 5 mM BHET. The optimum pH was determined at a pH range from 5.0 to 10.0. The following buffer systems were used: 50 mM C<sub>6</sub>H<sub>8</sub>O<sub>7</sub>-C<sub>6</sub>H<sub>9</sub>Na<sub>3</sub>O<sub>9</sub> buffer (pH 5.0–6.5); 50 mM Na<sub>2</sub>HPO<sub>4</sub>-NaH<sub>2</sub>PO<sub>4</sub> buffer (pH 6.0–8.0); 50 mM Tris-HCl buffer (pH 8.0–9.0); 50 mM Gly-NaOH buffer (pH 9.0–10.0). The degradation was terminated by adding one-third of the reaction volume of methanol. The enzyme assay for MHET followed the same procedure as described for BHET with slight modifications. For MHET assay, the 500 nM purified enzyme was added to 4 mL of the reaction system. The degradation was monitored by periodically taking

0.6 mL sample from the reaction mixture and rapidly terminating the reaction by adding one-third of the reaction volume of methanol. The sample was analyzed by HPLC.

PET degradation was carried out using PET-NP due to the low crystallinity of the material. PET-NP was cut into fixed size, and washed with 20% ethanol once followed by deionized water. The PET fragments were then incubated with 300 nM purified enzymes in 50 mM Gly-NaOH buffer (pH 9) at 30 °C. The degradation was monitored by HPLC as described above.

### 2.5. Thermal stability measurement

The thermal stabilities of *IsPETase<sup>Mut</sup>* and NusA-*IsPETase<sup>Mut</sup>* were measured by determining enzyme melting curves with protein thermal shift dye (Applied Biosystems) in qTOWER <sup>3</sup>G Real-Time PCR (Analytik Jena, Germany), the excitation wavelength was 470 nm and the emission wavelength was 520 nm. Briefly, the reaction was performed by mixing 5 µg enzyme with 1 x protein thermal shift dye in phosphate buffer (80 mM Na<sub>2</sub>HPO<sub>4</sub>, 40 mM NaCl, pH 7.5), and the enzyme melting curves were monitored by detecting the change in fluorescence at a temperature range from 25 °C to 95 °C at a rate of 0.5 °C·min<sup>-1</sup>. The melting temperature value (*T<sub>m</sub>*) is obtained by plotting the first derivative of the measured fluorescence trace versus temperature.

### 2.6. HPLC analysis

After centrifugation (13000×g for 15 min), the reaction mixtures were analyzed by using high performance liquid chromatography (waters e2695 coupled with a 2489 UV/Vis Detector) equipped with an Eclipse Plus-C18 column (5 µm, 4.6×250 mm). All analyses were performed at room temperature. The mobile phases were buffer A (0.1% trifluoroacetic acid water) and buffer B (methyl alcohol) at a flow rate of 0.8 mL/min. The flow phase gradually changes from 5% buffer B to 40% in 0 – 5 min, from 40% buffer B to 45% buffer B in 5 – 20 min. The analytes (BHET, MHET and TPA) were detected at 260 nm.

### 2.7. Kinetic analysis

For kinetic analysis, a two-step heterogeneous kinetic model based on substrate-limitation conditions was used [Scandola et al., 1998]. For this, a fixed surface area of PET-BP (*S<sub>0</sub>* = 1.44 cm<sup>2</sup>) was incubated with 0.6 mL of 50 mM Gly-NaOH buffer (pH 9). The reaction was triggered by adding a certain amount of enzyme (0 – 120 nM for *IsPETase<sup>Mut</sup>* and 0 – 500 nM for NusA-*IsPETase<sup>Mut</sup>*), and carried out at 30 °C for 48 h. The reaction was terminated by the addition of one-third of the reaction volume of methanol and analyzed by HPLC. Due to the low activity of the enzyme toward PET-BP with high crystallinity, initial hydrolysis rates were determined by end-point measurement. To ensure the accuracy of the experiments each measurement was carried out in triplicate. The obtained data were then fitted with the following two equations.

$$V_0 = k_2 S_0 \frac{KE}{K + E} \quad (1)$$

Equation (1) can be described as the following linearized expression:

$$\frac{S_0}{V_0} = \frac{1}{Kk_2E} + \frac{1}{k_2} \quad (2)$$

where *V<sub>0</sub>* is the initial rate of PET-BP hydrolysis, *S<sub>0</sub>* is the substrate surface concentration, *E* is the enzyme concentration, *K* is the adsorption constant, and *k<sub>2</sub>* is the hydrolysis constant.

### 2.8. Scanning electron microscopy (SEM)

After degradation, PET-NP was washed sequentially with 1% SDS for 30 min, 20% ethanol for 30 min, and deionized water for 30 min. The

samples were then dried at 50 °C for one night. The SEM was carried out using a Zeiss Gemini SEM 300 (Germany) with an electron beam intensity of 2.0 kV.

### 2.9. Differential scanning calorimetry (DSC)

DSC analysis of both PET-BP and PET-NP was performed using a differential scanning calorimeter (DSC 214 Polyma, Germany) as described before (Son et al., 2019). Briefly, the scans of both PET-BP and PET-NP were carried out at a temperature range of 0–300 °C with a speed of 10 °C/min for both cooling and heating. PET crystallinity was measured using the following equation:

$$\text{Crystallinity (\%)} = \frac{|\Delta H_m| - |\Delta H_c|}{\Delta H_m^{\circ}} \times 100 \quad (3)$$

where  $\Delta H_m^{\circ}$  is the heat of melting for a PET crystallinity of 100%, which is estimated to be 140.1 J·g<sup>-1</sup> (Ronkvist et al., 2009). Both the heat of melt ( $\Delta H_m$ ) and cold crystallization ( $\Delta H_c$ ) were determined by integrating the area of peaks (J·g<sup>-1</sup>).

### 2.10. NusA-*IsPETase<sup>Mut</sup>* structure analysis

The structure of NusA-*IsPETase<sup>Mut</sup>* was predicted by using AlphaFold2 that was installed and run as described at <https://github.com/deepmind/alphafold>. Five NusA-*IsPETase<sup>Mut</sup>* structures were output according to the model confidence ranking. The one with the highest confidence value was used for molecular docking analysis. Molecular docking calculations were performed using Autodock 4.2 with a model substrate of ethylene terephthalate (2PET) containing two repeating units. To generate pdbqt files for rigid and flexible receptors, flexible residues (Y605, T606, M769, W677, S678, D724, H755, N759, A798) were selected as docking Grid Box and molecular docking calculations were performed using Genetic Algorithm. In addition, *IsPETase<sup>Mut</sup>* and 2PET were also used in the same method for molecular docking calculations. The corresponding flexible residues (Y87, W159, S160, M161, W185, H237, S238, N241, A280) were chosen for the docking Grid Box. Finally, the binding free energy of the two proteins docked with 2PET was compared.

## 3. Results and discussion

### 3.1. General optimization of *IsPETase<sup>Mut</sup>* expression

The intracellular overexpression of *IsPETase<sup>Mut</sup>* (one of the most active mutants of *IsPETase* obtained so far) in *E. coli* was first explored by adopting the two commonly used expression vectors pBAD and pET30a, respectively. Because the inclusion bodies of overexpressed proteins are frequently formed due to incorrect folding of proteins containing disulfide bonds, a strain of *E. coli* shuffle T7 that was developed for the intracellular expression of proteins containing disulfide bonds was used as a host strain instead of the commonly used *E. coli* BL21 (DE3) because two functional disulfide bonds existed in *IsPETase<sup>Mut</sup>* (Lobstein et al., 2012). The results showed that the majority of the expressed *IsPETase<sup>Mut</sup>* was still in the form of inclusion bodies in the two expression systems even after conditions optimization, while the soluble fraction could only be visualized by Western blot analysis (Fig.S1). Thus, only 6 – 8 mg of purified *IsPETase<sup>Mut</sup>* was obtained from 1 L of culture medium. The results indicated that the existence of disulfide bonds in *IsPETase<sup>Mut</sup>* was not the main reason for its insoluble expression in *E. coli*.

In addition to the low soluble expression of *IsPETase<sup>Mut</sup>*, the inhibitory effect of IPTG on cell growth was also observed with an OD<sub>600</sub> of 1.2 – 1.5, resulting in only 6 ± 0.5 mg of purified *IsPETase<sup>Mut</sup>* per liter of culture medium. Therefore, ZYP self-inducing medium was applied. The results showed that the band related to the soluble fraction of *IsPETase<sup>Mut</sup>* on the SDS-PAGE gel could be visualized in this case. However, its

soluble expression level remained unimproved even after the optimization of induction temperatures (Fig. 1). By using ZYP self-inducing medium, the OD<sub>600</sub> of the recombinant cell culture in ZYP media could reach 2.0–2.5, resulting in 18 ± 1.8 mg purified *IsPETase<sup>Mut</sup>* per liter of culture medium. Thus, protein production by adopting ZYP self-inducing medium was 3-fold higher than that with IPTG induction.

### 3.2. Chaperone co-expression

Co-expression with chaperones has been frequently used to improve protein solubility in *E. coli* (Fatima et al., 2021; Gallardo et al., 2021). In order to investigate whether chaperone proteins could benefit the soluble expression of *IsPETase<sup>Mut</sup>*, three plasmids pGro7 (GroEL/ES), pKJE7 (Dnak/DnaJ/GrpE), and pTf16 (TF) were co-transformed with the plasmid carrying *IsPETase<sup>Mut</sup>* into *E. coli* shuffle-T7, respectively. The effects of co-expression chaperone on the soluble expression of *IsPETase<sup>Mut</sup>* were evaluated by SDS-PAGE analysis. The results showed that the overexpression of soluble *IsPETase<sup>Mut</sup>* was observed with GroEL/ES at 25 °C and 30 °C, while soluble expression of *IsPETase<sup>Mut</sup>* was failed at 18 °C (Fig. 2 and S2). Neither DnaK/DnaJ/GrpE nor TF chaperones promoted the improved soluble expression of *IsPETase<sup>Mut</sup>* at all tested conditions, which could be due to the lower soluble expression level of these two chaperones compared to that of GroEL/ES in *E. coli* (Fig. S2). Under the optimized condition (in ZYP medium at 25 °C), 75 ± 3.4 mg of purified *IsPETase<sup>Mut</sup>* (termed as *IsPETase<sup>Mut</sup>* (GroEL/ES)) was obtained from 1 L of culture, that was 12.5-fold higher than that of the expression of *IsPETase<sup>Mut</sup>*.

### 3.3. Fusion expression of *IsPETase<sup>Mut</sup>*

The fusion of a highly soluble tag to recombinant proteins represents another possibility to avoid inclusion bodies in *E. coli*. However, the effect of fusion tags on the production of soluble proteins is somehow unpredictable as its efficiency varies between different host strains and different types of proteins. To improve the soluble production of *IsPETase<sup>Mut</sup>* in *E. coli*, several frequently used fusion partners were thus adopted, including maltose-binding protein (Mbp), two hydrophilic tags

transcription termination anti-termination factor (NusA) and *E. coli* thioredoxin (TrxA), and small ubiquitin-related modifier (Sumo) (Kaur et al., 2018). For this, the N-terminal of the enzyme was fused to the C-terminal of the tested tags. The impact of these fusion tags on the soluble expression of *IsPETase<sup>Mut</sup>* conducted at varied temperatures was evaluated by SDS-PAGE analysis. Compared to the expression of native *IsPETase<sup>Mut</sup>*, a large improvement in the soluble production of *IsPETase<sup>Mut</sup>* was obtained with NusA protein, while the soluble fused *IsPETase<sup>Mut</sup>* bands were hardly visualized with the other tested tags (Fig. S3). Even no detectable purified enzymes were obtained from 1 L of culture after purification by His-tag affinity chromatography, indicating that the other three fusions failed to produce soluble *IsPETase<sup>Mut</sup>*. It is not surprised as the superior soluble expression ability of NusA over the other fusion tags has also been reported in the soluble expression of five proteins originated from the fish pathogen *Vibrio salmonicida* and the two related proteins from the mesophilic human pathogen *Vibrio cholerae* (Niiranen et al., 2007). Also, the solubility of human interleukin-6 (hIL-6) was much higher when it was fused with NusA than when it was fused with TrxA or ubiquitin (Ubi) (Kim et al., 2005).

Among all the tested temperatures, the highest soluble production of NusA-*IsPETase<sup>Mut</sup>* was obtained under the induction temperature of 20 °C (Fig. 3). The majority of the protein produced was insoluble at 25 °C and 30 °C, while the lowest expression level was observed at 16 °C (Fig. S4). Our results are consistent with previous reports where NusA increased soluble expression of proteins as long as they were expressed at 20–25 °C, and much less soluble expression when expressed at higher temperatures (Kohl et al., 2008; Korf et al., 2005).

Surprisingly, it was found that the His-tag affinity chromatography-purified NusA-*IsPETase<sup>Mut</sup>* appeared as two thick bands and one thin band on the SDS-PAGE gel with an apparent mass of approximately 85, 70 and 50 kDa, respectively (theoretical mass of NusA and *IsPETase<sup>Mut</sup>* is 55 and 28.6 kDa, respectively), while *IsPETase<sup>Mut</sup>* purified using the same strategy was revealed in only one major band of 28.6 kDa (Fig. 2). Moreover, the purification peak of the purified NusA-*IsPETase<sup>Mut</sup>*

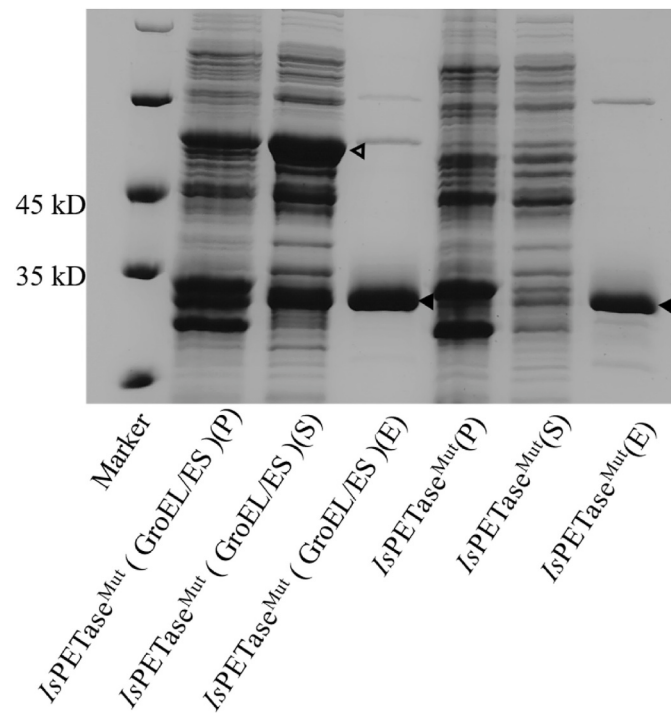


**Fig. 2.** SDS-PAGE analysis of the commonly expressed *IsPETase<sup>Mut</sup>* and the one co-expressed with GroEL/ES chaperone at 25 °C. P represents for pellet, S for supernatant, and E for purified enzyme. Hollow triangle and solid triangle represent the band of chaperone GroEL/ES and *IsPETase<sup>Mut</sup>*, respectively.

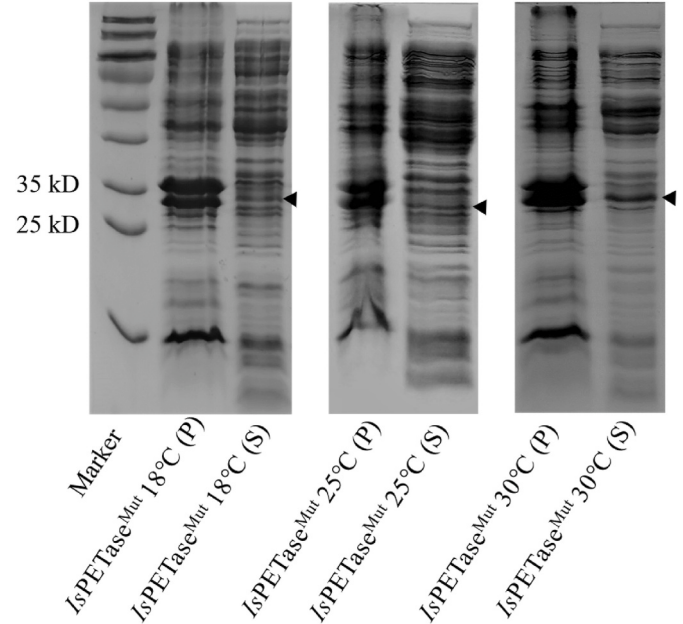


**Fig. 1.** SDS-PAGE analysis of the expression of recombinant *IsPETase<sup>Mut</sup>* in *E. coli* shuffle 7. The expression was conducted in ZYP self-induction media at temperatures of 18, 25, and 30 °C, respectively. P represents pellet and S for supernatant. *IsPETase<sup>Mut</sup>* band is marked with a solid triangle.

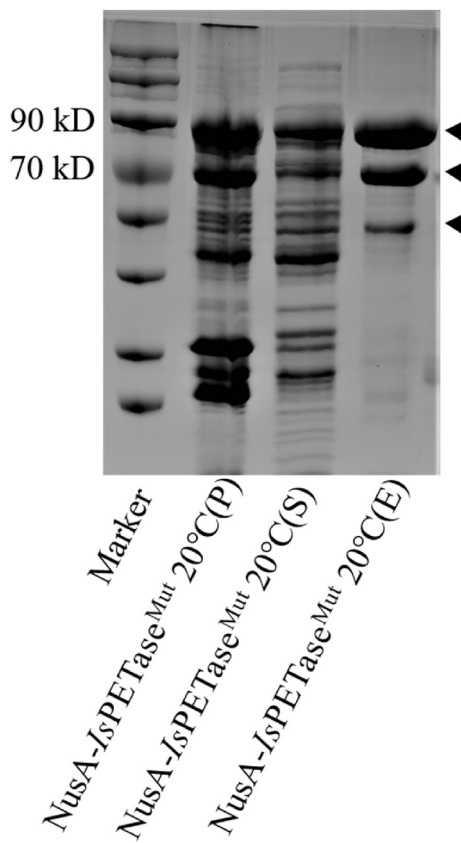


**Fig. 3.** SDS-PAGE analysis of the expression of NusA-IsPETase<sup>Mut</sup> in *E. coli* shuffle 7. The expression was conducted at 20 °C in ZYP self-induction media. P represents for pellet, S for supernatant, and E for purified enzyme obtained by using His-tag affinity chromatography. Multiple suspected NusA-IsPETase<sup>Mut</sup> bands are marked with solid triangles.

appeared as one symmetric peak, indicating that the obtained enzyme is quite pure (Fig. S5). To further investigate whether the other two bands were also related to NusA-IsPETase<sup>Mut</sup>, the purified NusA-IsPETase<sup>Mut</sup> was further analyzed using gel exclusion chromatography (Fig. S6A). The gel exclusion chromatography results showed that one major elution peak with a small shoulder was observed, which indicated that two proteins might be contained in this peak. However, it also implied that such a small difference in the elution volume of the two samples did not correlate well with the two major bands showing 15 kDa differences in mass. The collected gel exclusion chromatographic sample was then verified by SDS-PAGE and Native-PAGE. It showed that only one band of 85 kDa appeared in the Native-PAGE gel (Fig. S6C), while two major bands were still observed in the SDS-PAGE gel (Fig. S6B). Clearly, our results confirmed that at least these two major bands represent NusA-IsPETase<sup>Mut</sup>. The extra 70 kDa band might be caused by the structure interference of the fusion construct. Therefore, when cultured in ZYP medium at 20 °C, 80 ± 3.7 mg of purified NusA-IsPETase<sup>Mut</sup> was obtained from 1 L of culture. By taking into account of the mass of NusA protein, the valid production of pure IsPETase<sup>Mut</sup> is only 27.4 ± 1.3 mg, which is 4.6-fold higher than the expression of native IsPETase<sup>Mut</sup>.

The expression of IsPETase<sup>Mut</sup> using different expression systems in *E. coli* was summarized in Table 1. Both the chaperone co-expression and NusA fusion systems showed a large improvement in the soluble expression of IsPETase<sup>Mut</sup> in *E. coli*. It has been reported that in some cases the improved soluble expression of target proteins using the two strategies was mainly caused by preventing protein aggregation resulting from interactions between the hydrophobic regions of the proteins (Emamipour et al., 2019; Kaur et al., 2018; Lobstein et al., 2012; Tatkiewicz et al., 2015). Thus, the hydrophobicity of IsPETase<sup>Mut</sup>

**Table 1**

Summary of the expression of IsPETase<sup>Mut</sup> using different expression systems in *E. coli*.

Expression vectors	Host cells	Medium	Yields (mg·L <sup>-1</sup> )
pBAD-IsPETase <sup>Mut</sup>	<i>E. coli</i>	LB	8 ± 1.1
	Top10		
pET30-IsPETase <sup>Mut</sup>	<i>E. coli</i> shuffle-T7	LB	6 ± 0.5
pET30-IsPETase <sup>Mut</sup>	<i>E. coli</i> shuffle-T7	ZYP	18 ± 1.8
pET30-IsPETase <sup>Mut</sup> plus pGro7	<i>E. coli</i> shuffle-T7	ZYP	75 ± 3.4
pET30-NusA-IsPETase <sup>Mut</sup>	<i>E. coli</i> shuffle-T7	ZYP	80 ± 3.7

(GAP38373.1) was analyzed by using Expasy (<https://web.expasy.org/protscale/>), which is commonly used to calculate the hydrophobic or hydrophilic scale of proteins (Kyte and Doolittle, 1982; Rafeeq et al., 2021). Meanwhile, the hydrophobic property of its homologous enzyme TfCut2 (YP\_288944) was analyzed, the enzyme which showed high secreted expression in *E. coli* with up to 2.38 g per liter of culture medium (Chen et al., 2011; Su et al., 2012, 2013). The results showed that compared to TfCut2, IsPETase<sup>Mut</sup> contained three hydrophobic regions: residues 77 – 86, 103 – 113 and 195 – 215 (Fig. S7A), while TfCut2 with only two hydrophobic regions: residues 77 – 88 and 166 – 182 (Fig. S7B). Although other factors could not be excluded, such a hydrophobic property of IsPETase<sup>Mut</sup> might be one of the reasons for the fact that inclusion bodies were formed with the majority of expressed IsPETase<sup>Mut</sup> in *E. coli*.

### 3.4. Enzyme characterization

After systematic optimization of the expression of IsPETase<sup>Mut</sup> in *E. coli*, the activity of the purified enzymes was verified using both soluble fragment (BHET) and intact PET with different crystallinities (PET-NP with a crystallinity of 9.4% and PET-BP with a crystallinity of 17.9%) (Fig. S8). For BHET, the reaction was performed in phosphate buffer pH 7.5 (the optimum pH for the reaction) at 30 °C. The results showed that the enzymatic activities of IsPETase<sup>Mut</sup> and IsPETase<sup>Mut</sup> (GroEL/ES) were comparable with a specific activity of 2.99 ± 0.08 U·nmol<sup>-1</sup>, while that of NusA-IsPETase<sup>Mut</sup> was 1.93 ± 0.03 U·nmol<sup>-1</sup>, indicating that the chaperone GroEL/ES did not show any significant interruption on enzyme structure while facilitating the soluble expression of IsPETase<sup>Mut</sup>. With substrate PET-NP, the total released products of 3.5 ± 0.75 mM, 3.8 ± 0.52 mM, and 3.1 ± 0.3 mM were obtained for IsPETase<sup>Mut</sup>, IsPETase (GroEL/ES) and NusA-IsPETase<sup>Mut</sup>, respectively, after 48 h of incubation in 50 mM Gly buffer (pH 9.0) at 30 °C, while the total released products of 47.4 ± 3.3 μM, 47.6 ± 4.2 μM and 40.2 ± 0.3 μM were obtained with substrate PET-BP for the three enzymes, respectively. Although the three enzymes did not show a significant difference in the degradation efficiency of PET, they all displayed much lower activity toward PET with high crystallinity.

In addition, both NusA-IsPETase<sup>Mut</sup> and IsPETase<sup>Mut</sup> (GroEL/ES) were further characterized with aspects of thermostability, optimum temperature and optimum pH by using BHET as a model substrate. The thermal stability of NusA-IsPETase<sup>Mut</sup> and IsPETase<sup>Mut</sup> (GroEL/ES) was investigated using a thermofluor-based assay (Fig. S9). The two enzymes shared similar apparent melting temperature *T<sub>m</sub>* values of 59.1 and 58.6, respectively, indicating that no significant effect of the fusion NusA protein on the thermal stability of IsPETase<sup>Mut</sup> was produced. Moreover, both NusA-IsPETase<sup>Mut</sup> and IsPETase<sup>Mut</sup> (GroEL/ES) displayed a similar optimal temperature of 45 °C (Fig. S10A). NusA-IsPETase<sup>Mut</sup> displayed a slight shift of optimal pH range (6.5 – 8.0) compared to IsPETase<sup>Mut</sup> (GroEL/ES) (6.5 – 7.5) (Fig. S10B). NusA-IsPETase<sup>Mut</sup> showed approximately 1.5-fold improvement on enzyme activity with pH decreasing from 9.0 to 8.0, while the activity of IsPETase<sup>Mut</sup> (GroEL/ES) remained almost unchanged at this pH range. Such a catalytic property of NusA-IsPETase<sup>Mut</sup> might be gained by the structure interference of IsPETase<sup>Mut</sup> with NusA protein.

### 3.5. Kinetic analysis

Kinetic studies of both *IsPETase*<sup>Mut</sup> (GroEL/ES) and NusA-*IsPETase*<sup>Mut</sup> were performed by adopting a heterogeneous two-step kinetic model due to the insolubility of the PET substrate. In order to calculate accurately the surface area of PET, the substrate PET-BP instead of PET-NP was used. The hydrolysis of PET-BP catalyzed by the two enzymes was analyzed by HPLC analysis. The obtained data were fitted with equations (1) and (2) to obtain the kinetic parameters (Fig. 4). The results showed that the maximum initial rate ( $V_{max}$ ) of *IsPETase*<sup>Mut</sup> (GroEL/ES) was  $1.23 \pm 0.1 \mu\text{mol} \cdot \text{L}^{-1} \cdot \text{h}^{-1}$ , which was 1.43-fold higher than that of NusA-*IsPETase*<sup>Mut</sup> ( $0.86 \pm 0.01 \mu\text{mol} \cdot \text{L}^{-1} \cdot \text{h}^{-1}$ ), and the hydrolysis constant ( $k_2$ ) of *IsPETase*<sup>Mut</sup> (GroEL/ES) was 1.6-fold higher than that of NusA-*IsPETase*<sup>Mut</sup> (Table 2). In contrast, it was noticed that the adsorption constant ( $K$ ) of NusA-*IsPETase*<sup>Mut</sup> was 1.43-fold higher than that of *IsPETase*<sup>Mut</sup> (Table 2), indicating that the fused NusA protein increased the ability of *IsPETase*<sup>Mut</sup> to attach to PET. It is not surprising given that NusA has been shown to have chaperone activity, and its hydrophobic property may play a role in the increased adsorption constant ( $K$ ) of NusA-*IsPETase*<sup>Mut</sup>. It has been reported that the enhanced adsorptive ability of PETase could be gained by pre-incubating PET with hydrophobic proteins RolA and HGFI (Puspitasari et al., 2021). Moreover, fusion of carbohydrate-binding module (CBM), a polymer-binding

**Table 2**

Kinetic parameters of *IsPETase*<sup>Mut</sup> (GroEL/ES) and NusA-*IsPETase*<sup>Mut</sup> obtained from fitting analysis of Fig. 4

	$K$ ( $\text{nM}^{-1}$ )	$k_2$ ( $\text{nmol} \cdot \text{cm}^{-2} \cdot \text{h}^{-1}$ )
<i>IsPETase</i> <sup>Mut</sup> (GroEL/ES)	$0.069 \pm 0.006 \text{ nM}^{-1}$	$0.682 \pm 0.025 \text{ nmol cm}^{-2} \cdot \text{h}^{-1}$
NusA- <i>IsPETase</i> <sup>Mut</sup>	$0.099 \pm 0.007 \text{ nM}^{-1}$	$0.401 \pm 0.011 \text{ nmol cm}^{-2} \cdot \text{h}^{-1}$

domain that can adhere to a hydrophobic polymer surface, with PETase increased its hydrophobic binding, and consequently increased the hydrolysis efficiency of PETase (Dai et al., 2021; Ko et al., 2021; Ribitsch et al., 2015). Fusing auxiliary domains to the enzyme was proved to be a commonly used strategy to enhance the performance of PET hydrolytic enzymes. Taken together, the NusA fusion protein not only promoted the correct folding of *IsPETase*<sup>Mut</sup>, but also conferred new catalytic properties to the enzyme.

### 3.6. Biodegradation of PET bottle

To further investigate the performance of these enzymes in the long-term degradation of PET, PET-NP with low crystallinity was used. The degradation capacity of *IsPETase*<sup>Mut</sup> (GroEL/ES) and NusA-*IsPETase*<sup>Mut</sup> was evaluated by the measurement of the total released products of TPA,

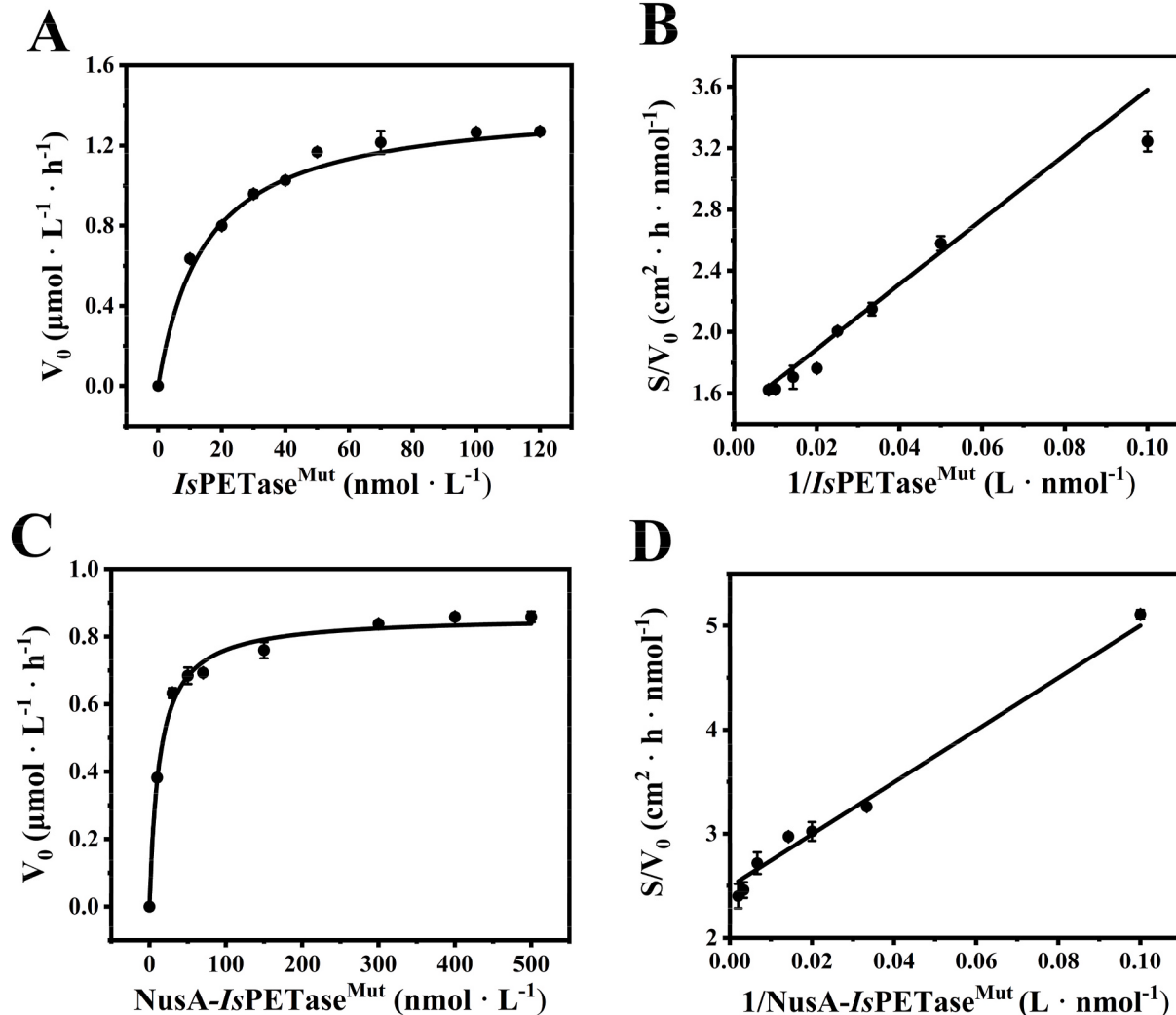


**Fig. 4.** Kinetic analysis of *IsPETase*<sup>Mut</sup> (GroEL/ES) and NusA-*IsPETase*<sup>Mut</sup> in the degradation of PET-BP. Experiments were performed with PET-BP at a fixed area of  $2.4 \text{ cm}^2 \cdot \text{mL}^{-1}$ . The solid lines were obtained by fitting the experimental data with equation (1) for panels A and C, and with equation (2) for panels B and D. Error bars are the mean of three independent measurements.

MHET, and BHET (Fig. S11). The results demonstrated that TPA and MHET are the main products and a very tiny amount of BHET was produced in all three cases. Such a product pattern was consistent with the results obtained from the other groups (Austin et al., 2018; Yoshida et al., 2016). The degradation behavior of *IsPETase<sup>Mut</sup>* (obtained by common expression method) and *IsPETase<sup>Mut</sup>* (GroEL/ES) is comparable as expected. However, it was observed that higher amount of MHET was accumulated for NusA-*IsPETase<sup>Mut</sup>* compared to the other two enzymes (*IsPETase<sup>Mut</sup>* and *IsPETase<sup>Mut</sup>* (GroEL/ES)). The production of TPA for NusA-*IsPETase<sup>Mut</sup>* was lower than that for the other two enzymes within 7 days (Fig. S11), while it reached at the same level afterwards, resulting in higher production of total released products after 4 days (Fig. 5A). After two weeks' degradation, 1.4-fold higher production with NusA-*IsPETase<sup>Mut</sup>* was achieved compared to that of *IsPETase<sup>Mut</sup>* and *IsPETase<sup>Mut</sup>* (GroEL/ES) (Fig. 5A). A similar trend was also obtained by weighting the substrate. A weight loss of  $19.6 \pm 2.3$  mg was obtained for PET-NP catalyzed by NusA-*IsPETase<sup>Mut</sup>*, which was 1.43-fold higher than that catalyzed by the other two enzymes (Fig. 5B). The enhanced degradation capacity of NusA-*IsPETase<sup>Mut</sup>* was further proved by SEM imaging (Fig. S12). Taken together, these results indicated that NusA-*IsPETase<sup>Mut</sup>* displayed a unique biodegradation behavior toward PET-NP compared to *IsPETase<sup>Mut</sup>* and *IsPETase<sup>Mut</sup>* (GroEL/ES), showing an application potential on the long-term biodegradation of PET-NP.

To gain more information related to the unique biodegradation behavior of NusA-*IsPETase<sup>Mut</sup>* toward PET-NP, the enzyme activity toward MHET was determined with both *IsPETase<sup>Mut</sup>* (GroEL/ES) and NusA-*IsPETase<sup>Mut</sup>*. The specific activities of  $3.48 \pm 0.1$  mU·nmol<sup>-1</sup> and  $1.02 \pm 0.18$  mU·nmol<sup>-1</sup> were obtained for the two enzymes, respectively. The results proved the fact that the accumulation of MHET with NusA-*IsPETase<sup>Mut</sup>* is more likely caused by the lower activity toward MHET than the other two enzymes (Fig. S13).

It was surprised that NusA-*IsPETase<sup>Mut</sup>* proceeded the long-term degradation of PET with a higher efficiency than the other two enzymes, although it had a lower hydrolysis constant. It was noticed that the optimum pH result of NusA-*IsPETase<sup>Mut</sup>* showed a higher relative activity when pH went down from 9 to lower when BHET was used as a model substrate (Fig. S10B). Therefore, we speculated that such a pH interference could lead to a higher released products of NusA-*IsPETase<sup>Mut</sup>* since the acidification of the reaction system upon the production of TPA was observed during the biodegradation of PET-NP in 50 mM Gly buffer at pH 9.0. Thus, the biodegradation of PET-NP was performed at a pH range from 8 to 9. However, it was not what we expected since the enzymatic activities of *IsPETase<sup>Mut</sup>* (GroEL/ES) and NusA-*IsPETase<sup>Mut</sup>*

were 58.5% and 51.8% of those at pH 9, respectively, when the reaction was performed at pH 8.5 (Fig. S14). Moreover, even no enzymatic reaction was observed at pH 8.0.

After excluding pH interference, the inhibition effect of TPA, the main product of the reaction, on the degradation efficacy of both *IsPETase<sup>Mut</sup>* (GroEL/ES) and NusA-*IsPETase<sup>Mut</sup>* toward PET-NP was investigated. Being the cosolvent of TPA, DMSO was proved to have a slight decrease effect on the degradation efficiency of NusA-*IsPETase<sup>Mut</sup>* with increasing the concentration of DMSO, but an opposite effect was observed for *IsPETase<sup>Mut</sup>* (Fig. S15A). Such a positive effect of DMSO on the conversion of amorphous PET film was observed with both wild-type *IsPETase* and its double mutant variant (Erickson et al., 2022).

When TPA was added to the reaction system, a clear inhibition effect was observed with the two enzymes. *IsPETase<sup>Mut</sup>* (GroEL/ES) showed a significant decrease in degradation capacity with increasing the concentration of TPA, while the inhibition trend of TPA on NusA-*IsPETase<sup>Mut</sup>* tended to go slowly with the concentration of TPA below 1 mM. However, the inhibition became more pronounced when the concentration of TPA reached to 2 mM with the relative activity of  $57.4 \pm 0.3\%$  for NusA-*IsPETase<sup>Mut</sup>* and  $41.2 \pm 1.8\%$  for *IsPETase<sup>Mut</sup>* (Fig. S15B). Till now, our results proved that both enhanced adsorption capacity toward PET and the reduced product inhibition effect of NusA-*IsPETase<sup>Mut</sup>* could contribute to the fact that NusA-*IsPETase<sup>Mut</sup>* performed long-term degradation of PET with a higher efficiency than the other two enzymes. However, other factors rather than those we explored could not be excluded and still need to be further investigated.

### 3.7. Structural analysis of NusA-*IsPETase<sup>Mut</sup>*

To reveal the nature of the observed catalytic properties of NusA-*IsPETase<sup>Mut</sup>*, the structure model of the enzyme was predicted by using AlphaFold2 that represents one of the most popular ones to enable the prediction with a high accuracy (Callaway, 2020; Gupta et al., 2021; Jumper et al., 2021; Tunyasuvunakool et al., 2021). The obtained model of NusA-*IsPETase<sup>Mut</sup>* with the highest confidence, indicating an average predicted local distance difference test (pLDDT) of 86.7 and the pLDDT of the structural regions were all above 90 (Fig. 6A). Thus, the structure prediction of NusA-*IsPETase<sup>Mut</sup>* is highly plausible since pLDDT > 90 is used as the cut-off point for a high precision (Tunyasuvunakool et al., 2021).

To demonstrate whether NusA affects the folding of *IsPETase<sup>Mut</sup>*, we chose root-mean-square deviation (RMSD) and TM-align (<https://zhanggroup.org/TM-align/>) for structural comparison of NusA-

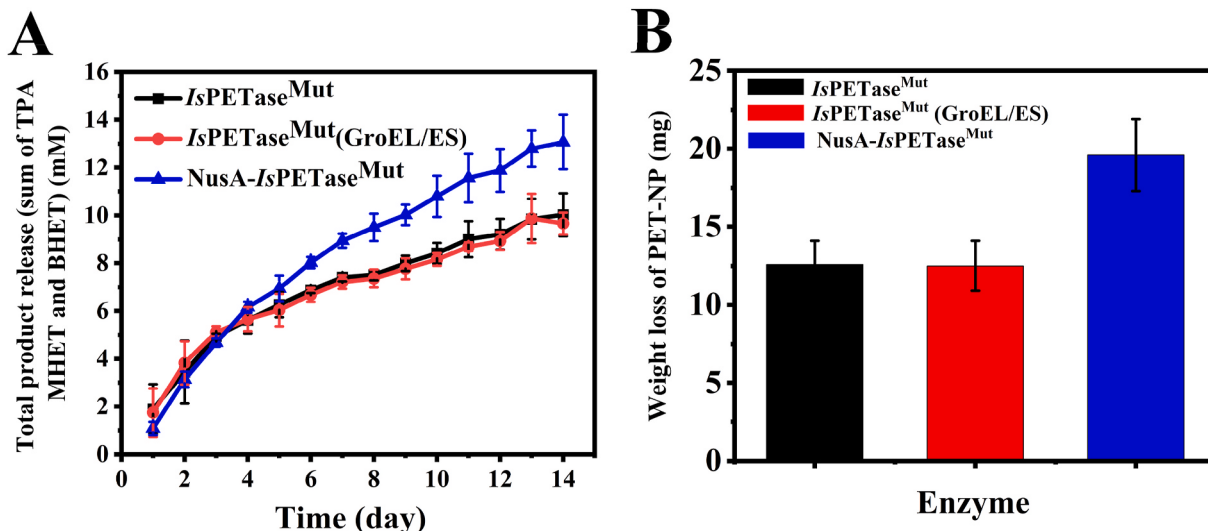


**Fig. 5.** Evaluation of PET-NP degradation capacity of three purified enzymes by measuring the total released product (A) and the corresponding weight loss (B). The error bars are the mean of three independent measurements.

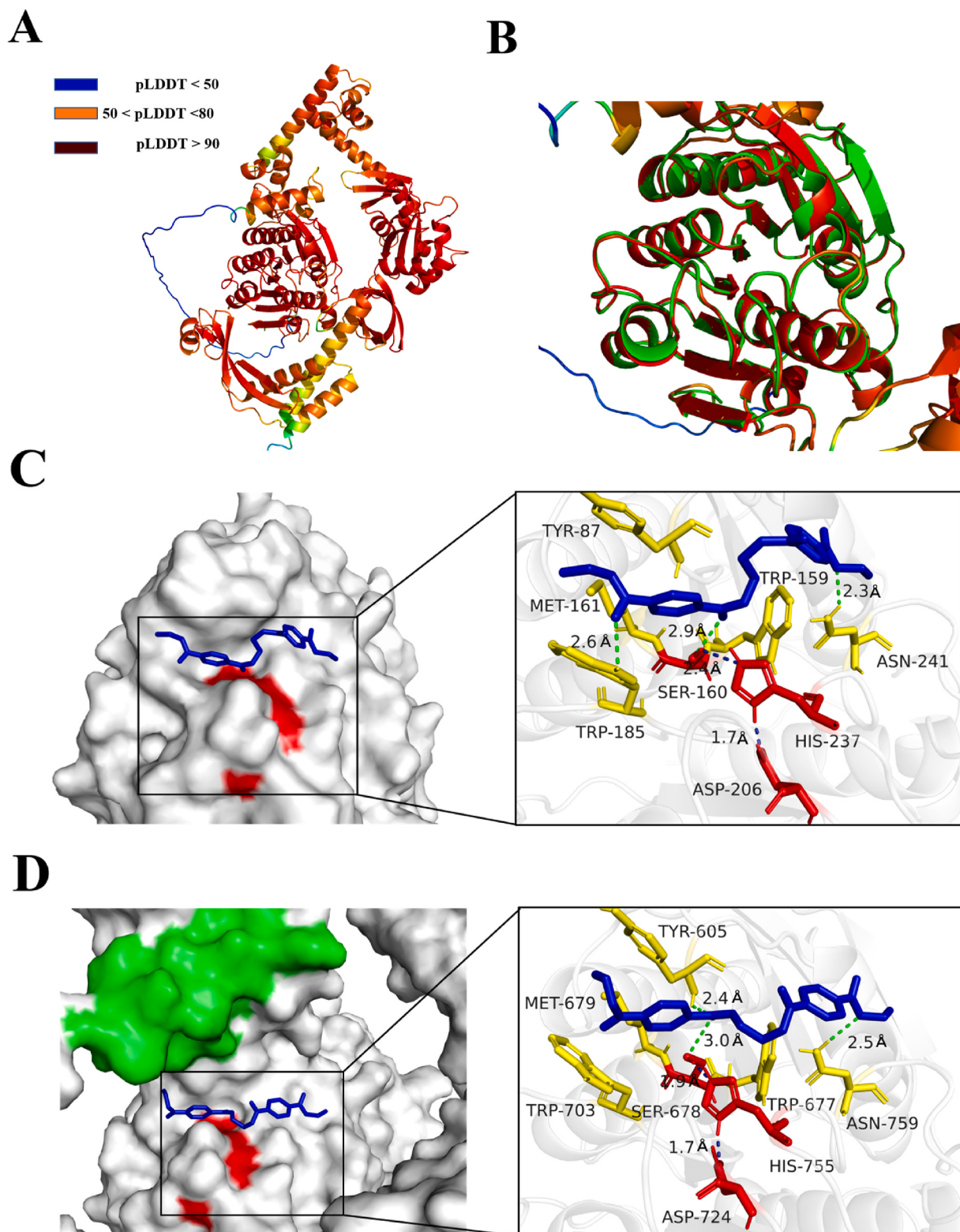


**Fig. 6.** Structural analysis of NusA-IsPETase<sup>Mut</sup>. (A) NusA-IsPETase<sup>Mut</sup> structure predicted by AlphaFold2 and the corresponding confidence analysis. (B) Structural superposition of NusA-IsPETase<sup>Mut</sup> and IsPETase<sup>Mut</sup>. Molecular docking analysis of IsPETase<sup>Mut</sup> (C) and NusA-IsPETase<sup>Mut</sup> (D) with 2PET. NusA residues of 486–501 are shown in green; residues located on the interface between the enzyme and 2PET are shown in yellow; 2PET in blue; catalytic triad in red. (For interpretation of the references to colour in this figure legend, the reader is referred to the Web version of this article.)

IsPETase<sup>Mut</sup> and IsPETase<sup>Mut</sup>. TM-align is an algorithm that allows fast and more accurate comparison of multiple protein structures, with a TM score of 0 indicating protein structures are unrelated and a TM score of 1 indicating an exact match (Dong et al., 2018; Kirchmair et al., 2008;

Zhang and Skolnick, 2005). The results showed that a RMSD of 0.348 and TM-score of 0.99601 were obtained in our case, suggesting that the NusA fusion did not show a significant interference on the overall structure of IsPETase<sup>Mut</sup> (Fig. 6B).

The predicted structure of NusA-*IsPETase*<sup>Mut</sup> together with the crystal structure of *IsPETase*<sup>Mut</sup> (PDB 6IJ6) were subsequently subjected to the analysis of hydrophobic surface distribution using the online software of Accessible Surface Area and Accessibility Calculation for Protein (ver. 1.2) (<http://cib.cfc.ocha.ac.jp/bitool/ASA/>). The results showed that the hydrophobic surface area of *IsPETase*<sup>Mut</sup> and NusA-*IsPETase*<sup>Mut</sup> was 1634.2 Å<sup>2</sup> and 9725.2 Å<sup>2</sup>, accounting for 16.8% and 21.6% of the overall area of the two enzymes, respectively, which indicated that the surface of NusA protein is more hydrophobic than *IsPETase*<sup>Mut</sup> alone (Fig. S16). Such a hydrophobic property of NusA could be accounted for the enhanced adsorption capacity of NusA-*IsPETase*<sup>Mut</sup> toward PET-NP.

To further investigate the differences in enzyme characteristics due to the fusion of NusA, we performed molecular docking calculations with both NusA-*IsPETase*<sup>Mut</sup> and *IsPETase*<sup>Mut</sup> by using 2PET as a model substrate. The docking results showed that 2PET bound with the two enzymes in a productive way, with hydrogen bonds formed between the catalytic residue Ser160 (Ser 678 in NusA-*IsPETase*<sup>Mut</sup>, 678 is the sum of the residue number of Ser160 in *IsPETase*<sup>Mut</sup> plus the total residue number of NusA 518) and the carbonyl group of 2PET. Moreover, the binding free energy of 2PET with NusA-*IsPETase*<sup>Mut</sup> (-5.03 kcat·mol<sup>-1</sup>) was a slightly higher than that of *IsPETase*<sup>Mut</sup> (-5.45 kcat·mol<sup>-1</sup>). It was observed that the binding mode of 2PET with the two enzymes was comparable with a slight difference of the binding orientation in the second benzene ring of 2PET, resulting in the loss of hydrogen bond forming between the oxygen of 2PET with the NH group of Trp 703 in NusA-*IsPETase*<sup>Mut</sup> (*IsPETase*<sup>Mut</sup> Trp 185 forms a 2.6 Å hydrogen bond with the oxygen of 2PET), but forming a new hydrogen bond between the backbone NH2 group of Tyr605 and carbonyl oxygen of 2PET (2.4 Å) (Fig. 6C and D). Moreover, the hydrogen bond formed between Asn 759 and 2PET (2.5 Å) in NusA-*IsPETase*<sup>Mut</sup> is weaker than that of Asn 241 with 2PET (2.3 Å) in *IsPETase*<sup>Mut</sup>, which might be due to the fact that the T-stacking interaction of Trp 159 with the first benzene ring of 2PET in *IsPETase*<sup>Mut</sup> is stronger than that in NusA-*IsPETase*<sup>Mut</sup> (Trp 677) (Fig. 6C and D). Taken together, these binding differences might account for the higher binding free energy of PET with NusA-*IsPETase*<sup>Mut</sup> over *IsPETase*<sup>Mut</sup>, thus, conferring new characteristics of NusA-*IsPETase*<sup>Mut</sup>.

#### 4. Conclusion

In this study, we systematically investigated the soluble production of *IsPETase*<sup>Mut</sup> in *E. coli* by adopting multiple strategies. Our results indicated that the formation of inclusion bodies of the overexpressed *IsPETase*<sup>Mut</sup> in *E. coli* is more likely due to protein aggregation resulting from interactions between the hydrophobic regions of the proteins rather than the existence of disulfide bond. Thus, a large improvement on the soluble expression of *IsPETase*<sup>Mut</sup> was obtained by adopting co-expression with chaperone GroEL/ES and fusion expression with NusA protein. Activity measurements proved that GroEL/ES promotes the correct folding of *IsPETase*<sup>Mut</sup>, while structure prediction analysis showed that NusA-*IsPETase*<sup>Mut</sup> displays a specific structure with *IsPETase*<sup>Mut</sup> encircled by the NusA protein, endowing the fusion enzyme new catalytic characteristics. The increased adsorption capacity of NusA-*IsPETase*<sup>Mut</sup> on PET and the reduced inhibition of the product could ensure a higher catalytic efficiency for long-term biodegradation of PET bottle. Taken together, our studies provide not only an efficient way to produce soluble recombinant *IsPETase*<sup>Mut</sup>, but also the kinetic investigation of the resulting enzymes on PET degradation, all of which could set a solid contribution to the biodegradation of PET.

#### Credit author statement

**Lizhu Aer:** Conceptualization, Investigation, Methodology, Data curation, Writing – original draft. **Qifa Jiang:** Validation. **Ijaz Gul:** Validation, Writing - review & revising. **Zixuan Qi:** Validation. **Juan Feng:** Conceptualization. **Lixia Tang:** Conceptualization, Supervision,

Funding acquisition, Writing – review & editing.

#### Funding

This work was supported by grants from the National Natural Science Foundation of China (No. 21673034) and Basic Research Program of Sichuan Science and Technology Foundation (2021YJ0223).

#### Declaration of competing interest

The authors declare that they have no known competing financial interests or personal relationships that could have appeared to influence the work reported in this paper.

#### Acknowledgements

This work was supported by grants from the National Natural Science Foundation of China (No. 21673034) and Basic Research Program of Sichuan Science and Technology Foundation, China (2021YJ0223). The authors also thank Prof. Peng Zhou for assistance with calculating protein hydrophobic surface.

#### Appendix A. Supplementary data

Supplementary data to this article can be found online at <https://doi.org/10.1016/j.enres.2022.113472>.

#### References

- Austin, H.P., et al., 2018. Characterization and engineering of a plastic-degrading aromatic polyesterase. Proc. Natl. Acad. Sci. U. S. A. 115, E4350–E4357. <https://doi.org/10.1073/pnas.1718804115>.
- Callaway, E., 2020. ‘It will change everything’: DeepMind’s AI makes gigantic leap in solving protein structures. Nature 588, 203–204. <https://doi.org/10.1038/d41586-020-03348-4>.
- Chae, Y., et al., 2018. Trophic transfer and individual impact of nano-sized polystyrene in a four-species freshwater food chain. Sci. Rep. 8, 1–11. <https://doi.org/10.1038/s41598-017-18849-y>.
- Chen, C.C., et al., 2018. Structural studies reveal the molecular mechanism of PETase. FEBS J. 285, 3717–3723. <https://doi.org/10.1111/febs.14612>.
- Chen, S., et al., 2011. Study on improvement of extracellular production of recombinant *Thermobifida fusca* cutinase by *Escherichia coli*. Appl. Biochem. Biotechnol. 165, 666–675. <https://doi.org/10.1007/s12010-011-9286-z>.
- Chen, Z., et al., 2020. Efficient biodegradation of highly crystallized polyethylene terephthalate through cell surface display of bacterial PETase. Sci. Total Environ. 709, 136138. <https://doi.org/10.1016/j.scitotenv.2019.136138>.
- Dai, L., et al., 2021. Enhancing PET hydrolytic enzyme activity by fusion of the cellulose-binding domain of cellobiohydrolase I from *Trichoderma reesei*. J. Biotechnol. 334, 47–50. <https://doi.org/10.1016/j.jbiotec.2021.05.006>.
- Danso, D., et al., 2018. New insights into the function and global distribution of polyethylene terephthalate (PET)-Degrading bacteria and enzymes in marine and terrestrial metagenomes. Appl. Environ. Microbiol. 84, e02773. <https://doi.org/10.1128/AEM.02773-17>, 17.
- Day, M., et al., 1982. Combustion and pyrolysis of poly(ethylene terephthalate). III. The effect of tris(2,3-dibromopropyl) phosphate on the products of pyrolysis. J. Appl. Polym. Sci. 27, 575–589. <https://doi.org/10.1002/app.1982.070270221>.
- Dong, R., et al., 2018. mTM-align: an algorithm for fast and accurate multiple protein structure alignment. Bioinformatics 34, 1719–1725. <https://doi.org/10.1093/bioinformatics/btx828>.
- Eberl, A., et al., 2009. Enzymatic surface hydrolysis of poly(ethylene terephthalate) and bis(benzoyloxyethyl) terephthalate by lipase and cutinase in the presence of surface active molecules. J. Biotechnol. 143, 207–212. <https://doi.org/10.1016/j.jbiotec.2009.07.008>.
- Emamipour, N., et al., 2019. Soluble expression of IGF1 fused to DsbA in SHuffle T7 strain: optimization of expression and purification by Box-Behnken design. Appl. Microbiol. Biotechnol. 103, 3393–3406. <https://doi.org/10.1007/s00253-019-09719-w>.
- Erickson, E., et al., 2022. Comparative performance of PETase as a function of reaction conditions, substrate properties, and product accumulation. ChemSusChem 15, e202101932. <https://doi.org/10.1002/cssc.202101932>.
- Fatima, K., et al., 2021. A review: molecular chaperone-mediated folding, unfolding and disaggregation of expressed recombinant proteins. Cell Biochem. Biophys. 79, 153–174. <https://doi.org/10.1007/s12013-021-00970-5>.
- Fecker, T., et al., 2018. Active site flexibility as a hallmark for efficient PET degradation by *I. Sakaiensis* PETase. Biophys. J. 114, 1302–1312. <https://doi.org/10.1016/j.bpj.2018.02.005>.

- Gallardo, P., et al., 2021. Reversible protein aggregation as cytoprotective mechanism against heat stress. *Curr. Genet.* <https://doi.org/10.1007/s00294-021-01191-2>.
- Gao, R., et al., 2021. Recent advances in the discovery, characterization, and engineering of poly(ethylene terephthalate) (PET) hydrolases. *Enzym. Microb. Technol.* 150. <https://doi.org/10.1016/j.enzmictec.2021.109868>.
- Gupta, M., et al., 2021. CryoEM and AI Reveal a Structure of SARS-CoV-2 Nsp 2, a Multifunctional Protein Involved in Key Host Processes. <https://doi.org/10.1101/2021.05.10.443524> bioRxiv.
- Hahladakis, J.N., et al., 2018. An overview of chemical additives present in plastics: migration, release, fate and environmental impact during their use, disposal and recycling. *J. Hazard Mater.* 344, 179–199. <https://doi.org/10.1016/j.jhazmat.2017.10.014>.
- Han, X., et al., 2017. Structural insight into catalytic mechanism of PET hydrolase. *Nat. Commun.* 8, 2106. <https://doi.org/10.1038/s41467-017-02255-z>.
- Herrero Acero, E., et al., 2011. Enzymatic surface hydrolysis of PET: effect of structural diversity on kinetic properties of cutinases from *Thermobifida*. *Macromolecules* 44, 4632–4640. <https://doi.org/10.1021/ma200949p>.
- Huang, X., et al., 2018. Tat-independent secretion of polyethylene terephthalate hydrolase PETase in *Bacillus subtilis* 168 mediated by its native signal peptide. *J. Agric. Food Chem.* 66, 13217–13227. <https://doi.org/10.1021/acs.jafc.8b05038>.
- Joo, S., et al., 2018. Structural insight into molecular mechanism of poly(ethylene terephthalate) degradation. *Nat. Commun.* 9, 1–12. <https://doi.org/10.1038/s41467-018-02881-1>.
- Jumper, J., et al., 2021. Highly accurate protein structure prediction with AlphaFold. *Nature* 596, 583–589. <https://doi.org/10.1038/s41586-021-03819-2>.
- Kaur, J., et al., 2018. Strategies for optimization of heterologous protein expression in *E. coli*: roadblocks and reinforcements. *Int. J. Biol. Macromol.* 106, 803–822. <https://doi.org/10.1016/j.ijbiomac.2017.08.080>.
- Kim, J.W., et al., 2020. Functional expression of polyethylene terephthalate-degrading enzyme (PETase) in green microalgae. *Microb. Cell Factories* 19, 97. <https://doi.org/10.1186/s12934-020-01355-8>.
- Kim, T.W., et al., 2005. Production of soluble human interleukin-6 in cytoplasm by fed-batch culture of recombinant *E.coli*. *Biotechnol. Prog.* 21, 524–531. <https://doi.org/10.1021/bp049645j>.
- Kirchmair, J., et al., 2008. Evaluation of the performance of 3D virtual screening protocols: RMSD comparisons, enrichment assessments, and decoy selection—what can we learn from earlier mistakes? *J. Comput. Aided Mol. Des.* 22, 213–228. <https://doi.org/10.1007/s10822-007-9163-6>.
- Ko, H., et al., 2021. A novel protein fusion partner, carbohydrate-binding module family 66, to enhance heterologous protein expression in *Escherichia coli*. *Microb. Cell Factories* 20, 232. <https://doi.org/10.1186/s12934-021-01725-w>.
- Kohl, T., et al., 2008. Automated production of recombinant human proteins as resource for proteome research. *Proteome Sci.* 6, 4. <https://doi.org/10.1186/1477-5956-6-4>.
- Korf, U., et al., 2005. Large-scale protein expression for proteome research. *Proteomics* 5, 3571–3580. <https://doi.org/10.1002/pmic.200401195>.
- Kyte, J., Doolittle, R.F., 1982. A simple method for displaying the hydrophobic character of a protein. *J. Mol. Biol.* 157, 105–132. [https://doi.org/10.1016/0022-2836\(82\)90515-0](https://doi.org/10.1016/0022-2836(82)90515-0).
- Liu, B., et al., 2018. Protein crystallography and site-direct mutagenesis analysis of the poly(ethylene terephthalate) hydrolase PETase from *Ideonella sakaiensis*. *Chembiochem* 19, 1471–1475. <https://doi.org/10.1002/cbic.201800097>.
- Lobstein, J., et al., 2012. SHuffle, a novel *Escherichia coli* protein expression strain capable of correctly folding disulfide bonded proteins in its cytoplasm. *Microb. Cell Factories* 11, 56. <https://doi.org/10.1186/1475-2859-11-56>.
- Meng, X., et al., 2021. Protein engineering of stable IsPETase for PET plastic degradation by Premuse. *Int. J. Biol. Macromol.* 180, 667–676. <https://doi.org/10.1016/j.ijbiomac.2021.03.058>.
- Moog, D., et al., 2019. Using a marine microalga as a chassis for polyethylene terephthalate (PET) degradation. *Microb. Cell Factories* 18, 1–15. <https://doi.org/10.1186/s12934-019-1220-z>.
- Niiranen, L., et al., 2007. Comparative expression study to increase the solubility of cold adapted *Vibrio* proteins in *Escherichia coli*. *Protein Expr. Purif.* 52, 210–218. <https://doi.org/10.1016/j.pep.2006.09.005>.
- Pabortsava, K., Lampitt, R.S., 2020. High concentrations of plastic hidden beneath the surface of the Atlantic Ocean. *Nat. Commun.* 11, 1–11. <https://doi.org/10.1038/s41467-020-17932-9>.
- Puspitasari, N., et al., 2021. Class I hydrophobins pretreatment stimulates PETase for monomers recycling of waste PETs. *Int. J. Biol. Macromol.* 176, 157–164. <https://doi.org/10.1016/j.ijbiomac.2021.02.026>.
- Rafeeq, C.M., et al., 2021. Characterisation and comparative analysis of hydrophobin isolated from *Pleurotus floridanus* (PfH). *Protein Expr. Purif.* 182, 105834. <https://doi.org/10.1016/j.pep.2021.105834>.
- Ribitsch, D., et al., 2015. Enhanced cutinase-catalyzed hydrolysis of polyethylene terephthalate by covalent fusion to hydrophobins. *Appl. Environ. Microbiol.* 81, 3586–3592. <https://doi.org/10.1128/AEM.04111-14>.
- Rochman, C.M., et al., 2013. Policy: classify plastic waste as hazardous. *Nature* 494, 169–171. <https://doi.org/10.1038/494169a>.
- Ronkvist, Å.M., et al., 2009. Cutinase-catalyzed hydrolysis of poly(ethylene terephthalate). *Macromolecules* 42, 5128–5138. <https://doi.org/10.1021/ma9005318>.
- Seo, H., et al., 2019. Production of extracellular PETase from *Ideonella sakaiensis* using sec-dependent signal peptides in *E. coli*. *Biochem. Biophys. Res. Commun.* 508, 250–255. <https://doi.org/10.1016/j.bbrc.2018.11.087>.
- Shi, L., et al., 2021. Enhanced extracellular production of IsPETase in *Escherichia coli* via engineering of the pelB signal peptide. *J. Agric. Food Chem.* 69, 2245–2252. <https://doi.org/10.1021/acs.jafc.0c07469>.
- Skoczinski, P., et al., 2021. Current status and future development of plastics: solutions for a circular economy and limitations of environmental degradation. *Methods Enzymol.* 648, 1–26. <https://doi.org/10.1016/bs.mie.2020.11.001>.
- Son, H.F., et al., 2019. Rational protein engineering of thermo-stable PETase from *Ideonella sakaiensis* for highly efficient PET degradation. *ACS Catal.* 9, 3519–3526. <https://doi.org/10.1021/acscatal.9b00568>.
- Su, L., et al., 2012. Extracellular overexpression of recombinant *Thermobifida fusca* cutinase by alpha-hemolysin secretion system in *E. coli* BL21(DE3). *Microb. Cell Factories* 11, 8. <https://doi.org/10.1186/1475-2859-11-8>.
- Su, L., et al., 2013. Extracellular location of *Thermobifida fusca* cutinase expressed in *Escherichia coli* BL21(DE3) without mediation of a signal peptide. *Appl. Environ. Microbiol.* 79, 4192–4198. <https://doi.org/10.1128/AEM.00239-13>.
- Tatkiewicz, W., et al., 2015. Methods for characterization of protein aggregates. *Methods Mol. Biol.* 1258, 387–401. [https://doi.org/10.1007/978-1-4939-2205-5\\_22](https://doi.org/10.1007/978-1-4939-2205-5_22).
- Tunyasuvanakool, K., et al., 2021. Highly accurate protein structure prediction for the human proteome. *Nature* 596, 590–596. <https://doi.org/10.1038/s41586-021-03828-1>.
- Wang, N., et al., 2020. Enhancing secretion of polyethylene terephthalate hydrolase PETase in *Bacillus subtilis* WB600 mediated by the SPamy signal peptide. *Lett. Appl. Microbiol.* 71, 235–241. <https://doi.org/10.1111/lam.13312>.
- Wei, R., Zimmermann, W., 2017. Microbial enzymes for the recycling of recalcitrant petroleum-based plastics: how far are we? *Microb. Biotechnol.* 10, 1308–1322. <https://doi.org/10.1111/1751-7915.12710>.
- Xi, X., et al., 2021. Secretory expression in *Bacillus subtilis* and biochemical characterization of a highly thermostable polyethylene terephthalate hydrolase from bacterium HR29. *Enzym. Microb. Technol.* 143, 109715. <https://doi.org/10.1016/j.enzmictec.2020.109715>.
- Yoshida, S., et al., 2016. A bacterium that degrades and assimilates poly(ethylene terephthalate). *Science* 351, 1196–1199. <https://doi.org/10.1126/science.aad6359>.
- Zhang, X., et al., 2018. Catalysis as an enabling science for sustainable polymers. *Chem. Rev.* 118, 839–885. <https://doi.org/10.1021/acs.chemrev.7b00329>.
- Zhang, Y., Skolnick, J., 2005. TM-align: a protein structure alignment algorithm based on the TM-score. *Nucleic Acids Res.* 33, 2302–2309. <https://doi.org/10.1093/nar/gki524>.
- Zope, V.S., Mishra, S., 2008. Kinetics of neutral hydrolytic depolymerization of PET (polyethylene terephthalate) waste at higher temperature and autogenous pressures. *J. Appl. Polym. Sci.* 110, 2179–2183. <https://doi.org/10.1002/app.28190>.